HERON contains contributions based mainly on research work performed in I.B.B.C. and STEVIN and related to strength of materials and structures and materials science.

Jointly edited by:

STEVIN-LABORATORY
of the Department of
Civil Engineering of the
Delft University of Technology
Delft, The Netherlands
and
I.B.B.C. INSTITUTE TNO
for Building Materials
and Building Structures,
Rijswijk (ZH), The Netherlands.

HERON vol. 21
1976
no. 4

Contents

EXPERIMENTAL INVESTIGATION OF THE EFFECT OF VARYING THE REINFORCEMENT UPON THE BEHAVIOUR OF CIRCULAR SLABS

A. L. Bouma
H. van Koten
F. G. Koch
J. Meek

NOTATION

r, t, w	cylindrical co-ordinates
w	deflection perpendicular to middle plane of slab
w_{max}	deflection at centre of circular slab
h_{tot}	total depth of slab
d_r, d_t	distance from centroid of reinforcement to extreme tensile fibre of concrete (in radial and in tangential direction)
v_r, v_t, v	Poisson's ratio
h_r, h_t	effective depth of concrete section in radial and in tangential direction
R	radius of circular slab
A	cross-sectional area of reinforcement
ϕ_t	diameter of reinforcing bars in tangential direction
ϕ_r	diameter of reinforcing bars in radial direction
ω_r, ω_t	reinforcement percentages in radial and in tangential direction $(A/h \times 100\%)$
M_r, M_t	bending moments per unit length in radial and in tangential direction
$M_{r,p}, M_{t,p}$	plastic moments in radial and in tangential direction
q_r, q_t	shear force per unit length in radial and in tangential direction
$M_{r,s}$	cracking moment in radial direction of concrete section
$M_{t_{max}}$	maximum moment that can be resisted in tangential direction (in the presence of normal compressive stresses)
k_r, k_t	flexural rigidity of slab in radial and in tangential direction
α	$\sqrt{k_t/k_r}$
P	concentrated load
q	uniformly distributed load
P_u, q_u	collapse loads
σ_b	flexural strength of concrete
σ_{sp}	splitting strength of concrete
σ'_w	cube strength (average) of concrete
σ'_{bu}	maximum compressive stress in concrete at collapse
σ_{ae}	yield stress in steel

Experimental investigation of the effect of varying the reinforcement upon the behaviour of circular slabs

Report on experimental research carried out in the Stevin Laboratory of the Technological University of Delft by the two-last-mentioned authors for obtaining the Diploma in Civil Engineering.

1 Introduction

The analysis of reinforced concrete slabs is usually based on the linear elastic theory or on the yield-line theory. So long as a concrete slab is uncracked, the bending moment distribution in it will be in reasonably good agreement with the results of the linear elastic theory applied to an isotropic plate. The yield-line theory gives the value of the collapse load, provided that the correct collapse mechanism has been assumed. This theory does not, however, give the values of deformations or the displacements associated with the collapse load. For one and the same value of the collapse load these displacements may vary considerably, depending on the pattern of reinforcement employed, in the choice of which the designer has a certain amount of freedom.

With increasing cracking the rigidity of a slab will diminish. Under such conditions the rigidity will depend mainly on the quantity of reinforcement provided. However, if the reinforcement is not the same in different directions, the slab will have become anisotropic and its bending moment distribution will differ from that in an isotropic slab. If there are big differences in the percentages of reinforcement, the distribution of the moments may be considerably altered in consequence. In the case of the circular slab, for example, anisotropy may give rise to entirely different results. Thus, the well-known singularity under a point load may disappear, while under uniformly distributed load the moments at the centre may become zero.

This modified bending moment distribution may result in another – a different – cracking pattern which may finally develop into the yield-line pattern of the collapse mechanism. The object of the research reported here was to study this development and more particularly to investigate the effect of anisotropy in the cracked state – due to different reinforcement percentages – on the rigidity (or the displacements), on the collapse mechanism and on the magnitude of the collapse load.

To this end, model investigations were carried out *) on ten circular slabs made of reinforced micro-concrete (scaled-down concrete for models), six of which were subjected to a concentrated load applied at the centre and four to a uniformly distributed load.

*) in the Stevin Laboratory

The circular slab was chosen because of its remarkable behaviour with regard to anisotropy and because, with its axial symmetry, the principal stress directions coincide with the reinforcement directions and the torsional stiffness has no effect.

The concentrated load acting at the centre of the circular slab moreover constitutes a basic case by means of which the effect of concentrated loads on slabs can be investigated independently of the slab boundary conditions.

The behaviour of the slabs was found to be suitably amenable to investigation and to give some surprising results. Thus, for instance, in the case of uniformly distributed load it was found that anisotropy could lead to a different collapse mechanism with a lower collapse load than that occurring in the case of isotropy. Also, an insight into the effect of the membrane forces was obtained. These forces may give rise to different collapse mechanisms with higher values of the collapse load. With the concentrated load, however, the phenomenon of punching shear occasionally altered the situation in that a collapse mechanism based on yield lines then did not suffice.

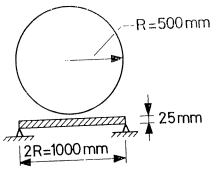

Fig. 1. Dimensions of slabs.

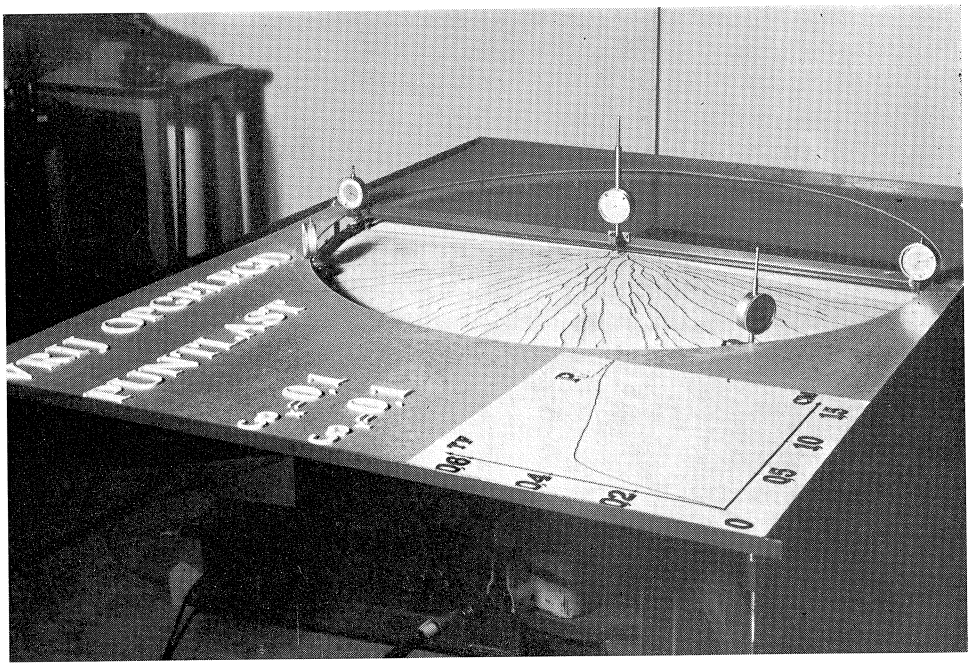

Fig. 2. Test set-up.

uniformly distributed load			point load		
slab	ω_t	ω_r	slab	ω_t	ω_r
01	1	1	11	1	1
02	1	0,5	12	1	0,5
03	1	0,25	13 A	0,5	1
04	0,5	1	13 B	0,5	1
			14	1	0,25
			15	$\omega_{x\ 0,75}$	$\omega_{y\ 0,75}$ (orthogonal mesh)

Fig. 3. Percentages of reinforcement ($\omega = A/h \times 100\%$) in the slabs under investigation.

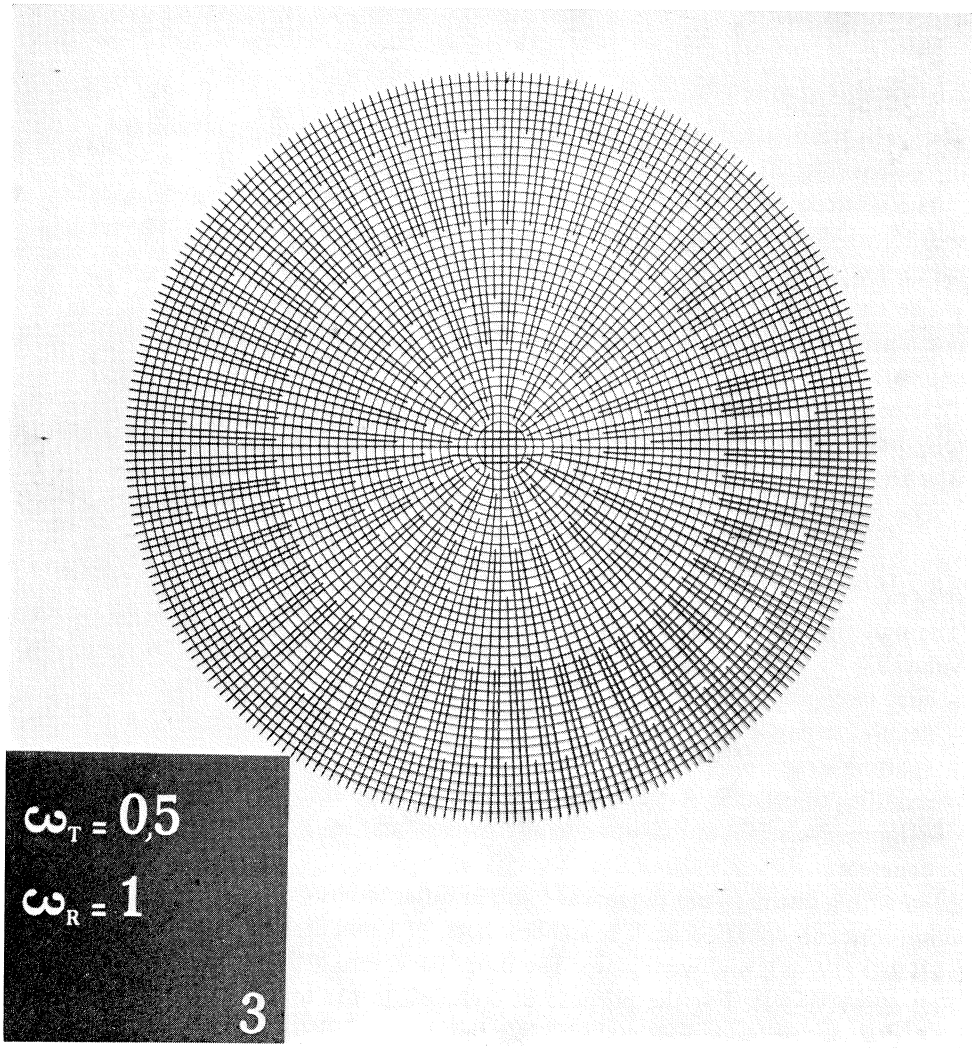

Fig. 4. Axially symmetrical reinforcement.

Apart from this punching shear effect the phenomena were found to be capable of explanation on the basis of simple considerations; this is also true of the effect of the membrane forces. And although we are here concerned only with a slab of simple shape, the results and the considerations associated with them are applicable also tot other slab shapes, while the conclusions are of wider scope.

2 Model research

The tests for this research were performed on circular reinforced concrete slabs of 100 cm diameter and 2.5 cm thickness (Fig. 1) which were loaded by a point load or uniformly distributed load. Fig. 2 shows the experimental set-up for the slab tested under point load.

2.1 *Details of the slabs*

Ten slabs were tested; these were provided with the following percentages of reinforcement (Fig. 3).

The reinforcement was disposed in an axially symmetrical arrangement, except in slab 15, which had an orthogonal mesh. The reinforcement was woven. The tangential bars were joined by means of butt welds (Fig. 4).

The radial reinforcement (see Fig. 4) comprised some discontinuities, which were introduced in order to approximate as closely as possible to a constant reinforcement percentage.

After testing, the thickness of the slabs and the concrete cover to the two sets of reinforcement (radial and tangential) were determined in three places and the average was then calculated (Fig. 21).

The details of the slabs are schematically summarized in Appendix A.

2.2 *Materials*

The material properties of the *concrete* were characterized by the following average values:

- cube strength $\sigma'_w = 50.0$ N/mm^2
- flexural strength $\sigma_b = 6.0$ N/mm^2
- splitting strength $\sigma_{sp} = 4.2$ N/mm^2
- modulus of elasticity (at origin of stress-strain diagram) $E'_b = 34400$ N/mm^2
- compressive strain at maximum compressive stress in concrete $\varepsilon'_{bu} = 0.2\%$

Steel with a distinct yield range was used, in order to ensure that no fracturing of the reinforcement would occur. The smallest bars, of 1 mm diameter, were of steel grade FeB 240 HW-NL and were plain. The other bars were deformed bars of steel grade FeB 400 HW-NR. For the purpose of comparison the tangential reinforcement in slab 13B was of grade FeB 400 HK-NR instead of FeB 400 HW-NR.

The materials used and the material constants are fully presented in Appendix B.

2.3 *Testing procedure*

In order to have hinged (freely rotatable) bearings under the slabs, the latter extended 10 mm beyond the bearings (Fig. 5). To prevent this outermost circumferential portion of the slab from acting as a compression ring, it was provided with saw cuts extending radially inwards at the rocker columns forming the bearings (Fig. 5).

The *point load* was applied by means of a jack, the force being transmitted through a punch (75 mm diameter) to the slab (Fig. 6).

The *uniformly distributed load* was applied with the aid of air pressure, which was exerted by an inflated rubber bag enclosed in a steel casing. This load, like the point load, acted on the underside of the test slab (Fig. 7).

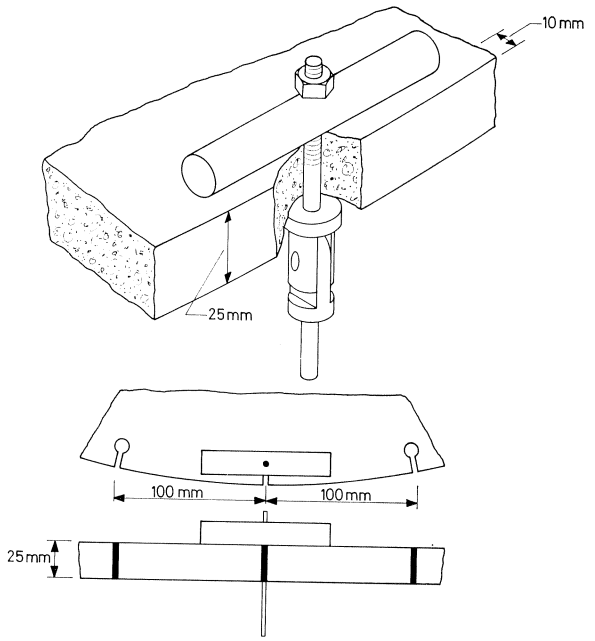

Fig. 5. Detail of bearing with hinge and rocker column.

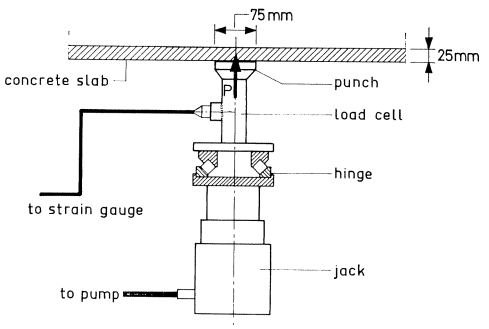

Fig. 6. Method of applying the point load.

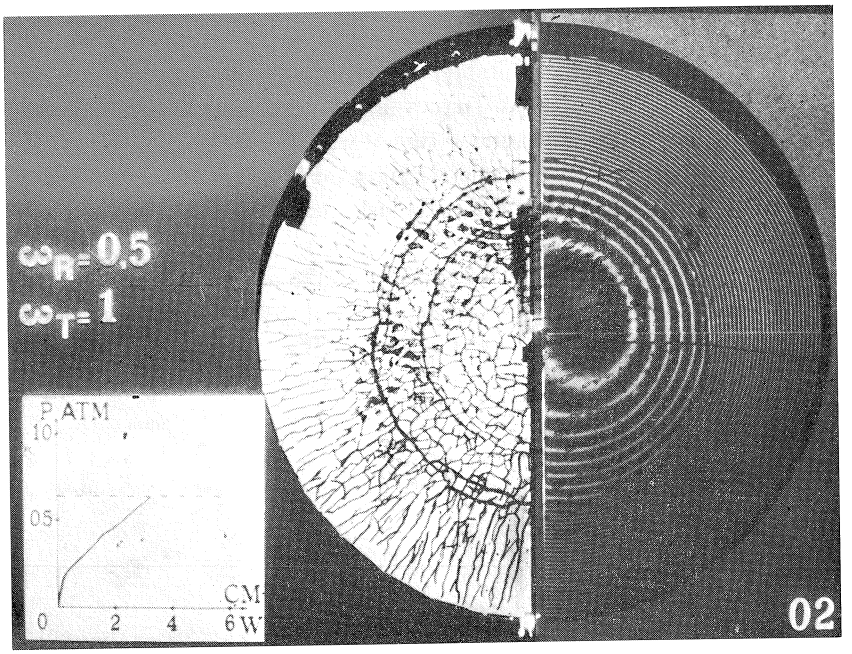

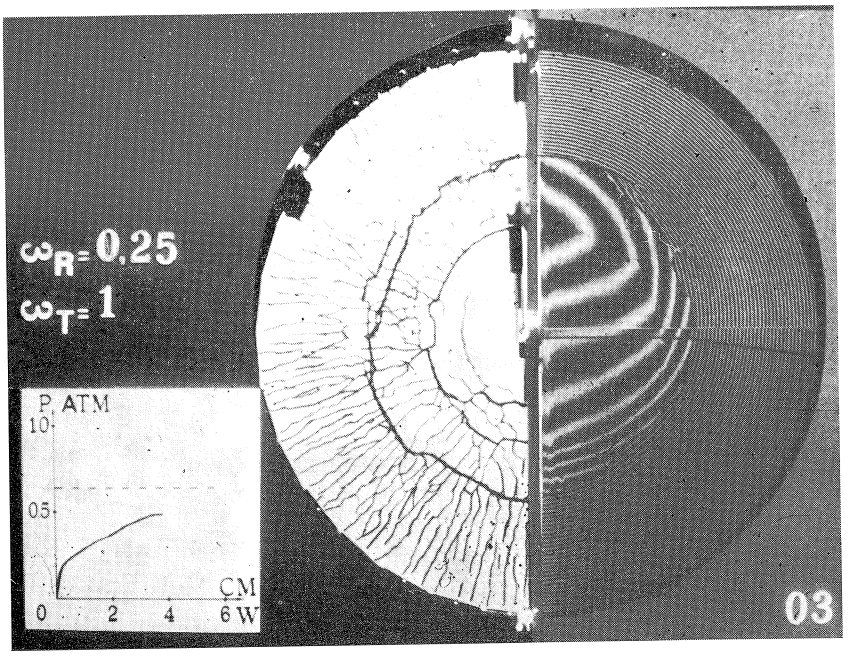

Fig. 8, Fig. 9. Collapse patterns of slabs 02 and 03; freely supported, loaded over entire area (uniformly distributed load).

Note Collapse pattern of slab 04, pyramid-shaped: $\omega_t = 0.5 \quad \omega_r = 1$

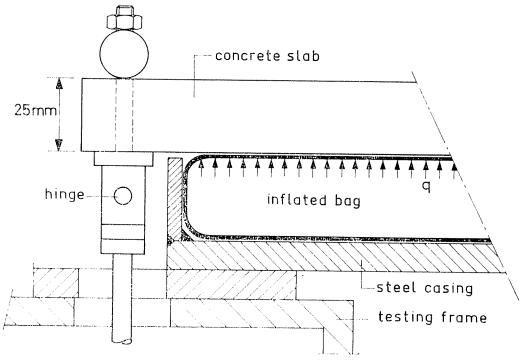

Fig. 7. Detail of bearing and method of applying the uniformly distributed load.

The *deflection* of the slab was measured at several points by means of dial gauges. Furthermore, with the aid of the shadow moiré method an overall picture of the distribution of the deflections of the slab was obtained. Half a slab was used for this purpose. The cracking pattern was drawn in the other half (Figs. 8 and 9).

At each stage of loading, the deflection behaviour and the developing of the cracking pattern were recorded photographically.

3 Behaviour of the slabs under point load or uniformly distributed load

3.1 *General*

The load-deflection diagrams of the slabs are presented in Fig. 10 (point load) and Fig. 11 (uniformly distributed load).

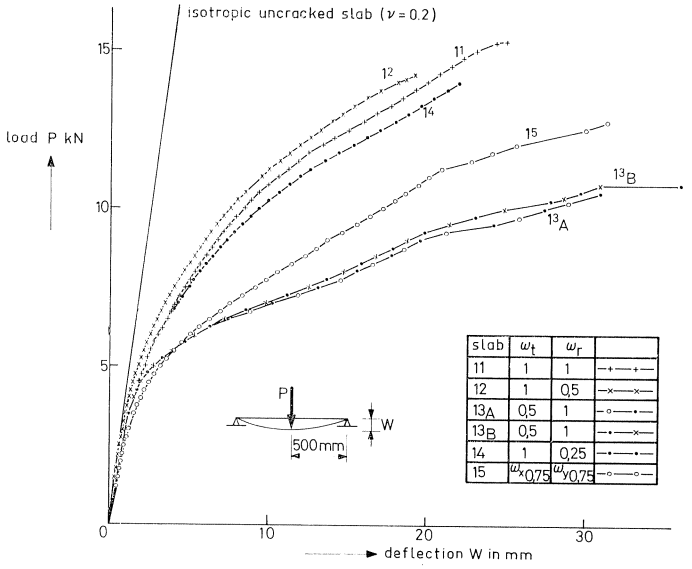

Fig. 10. Assembled test results of the circular slabs.

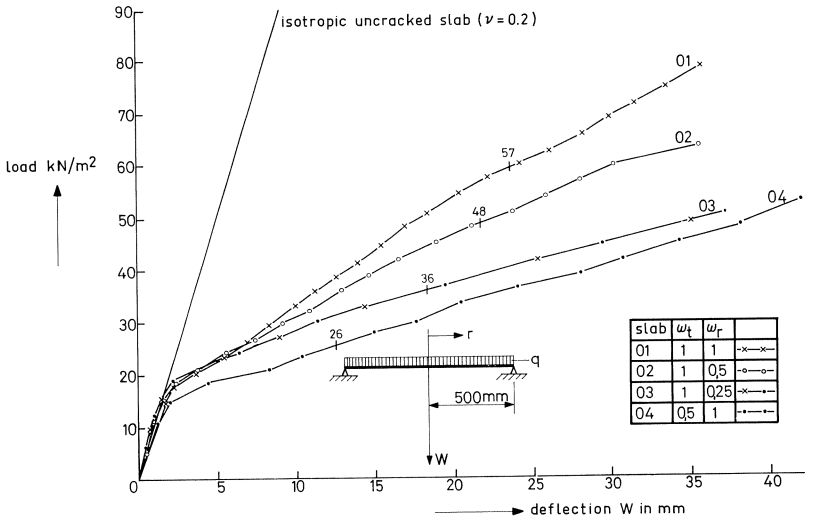

Fig. 11. Assembled test results.

With increasing load the diagram at first conforms to the straight line calculated for an uncracked isotropic slab. As a result of the cracking moment in the tangential and the radial direction being exceeded, however, the load-deflection diagram deviates from that line: the slab becomes less rigid and develops behaviour which may vary greatly from one slab to another. With further load increase, the zone where cracking occurs will gradually spread, so that the slab loses more and more of its rigidity.

Also, with increasing load, yielding of the reinforcement will occur, and the zones where this occurs will increase and spread until a mechanism develops which causes the slab to collapse. During the loading process the slab will thus comprise various zones which differ from one another in their flexural rigidity.

The bilinear moment-curvature diagram in Fig. 12 has been adopted for determining the flexural rigidity values.

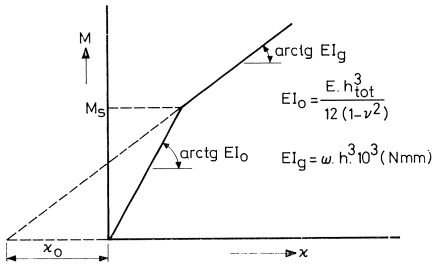

Fig. 12. Moment-curvature relationship for reinforced concrete.

In the uncracked state the effect of the reinforcement on the flexural rigidity is neglected and the following expression is adopted:

$$EI_0 = Eh_{tot}^3/12(1-\nu^2) \qquad [\text{Nmm}]$$

In the cracked state the flexural rigidity has experimentally been shown to be proportional to the percentage of reinforcement (ω) in accordance with the formula:

$$EI_g = \omega \cdot h^3 \cdot 10^3 \qquad [\text{Nmm}]$$

In the cracked state the reinforcement percentage is therefore representative of the flexural rigidity.

3.2 *Slabs loaded by a point load*

From Fig. 10 it is evident that the slabs 11, 12 and 14 are much alike as regards strength and rigidity. These slabs had the same tangential reinforcement percentage (ω_t), but differed greatly in their radial reinforcement percentage (ω_r). It appears that in a slab loaded by a point load the radial reinforcement has little effect on the behaviour of the slab.

On the other hand, halving the tangential reinforcement percentage ω_t (slab 11 → slab 13A) has a considerable effect on the strength and rigidity of the slab. Slab 15, which was reinforced with an orthogonal mesh, served for comparison.

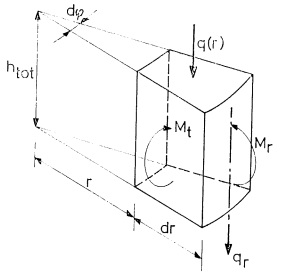

Fig. 13. Forces acting on a slab element.

In the following treatment of the subject the effect of anisotropy on the behaviour of the slab will be illustrated with theoretical results. (The background of the theory is dealt with in Appendix C.)

Fig. 13 shows an elementary portion of the slab with the forces acting on it.

For a slab supported on hinge-type bearings and subjected to a point load it was investigated how the magnitude of the ratio of tangential to radial flexural rigidity $\alpha(=\sqrt{k_t/k_r})$ affects the deflections and bending moments.

POINT LOAD

flexural rigidities	$\alpha = \sqrt{\frac{K_t}{K_r}}$	deflection at centre of slab (W)	W in %
$K_r = 2K$ $K_t = 2K$	1	$0.09375 \frac{P.R^2}{\pi K}$	100
$K_r = K$ $K_t = 2K$	$\sqrt{2}$	$0.1025 \frac{PR^2}{\pi K}$	109
$K_r = 2K$ $K_t = K$	$1/2\sqrt{2}$	$0.1625 \frac{PR^2}{\pi K}$	173

Fig. 14. Theoretical effect of k_t and k_r on deflection at the centre of the slab.

The deflections at the centre of the slab for three values of α are indicated in Fig. 14.

It appears from this that halving the radial flexural rigidity has only little effect on the deflection at the centre of the slab; on the other hand, halving the tangential flexural rigidity has a considerable effect. This result is in agreement with the experimental evidence.

In Fig. 15 the radial and the tangential bending moments are presented for various values of α.

$$M_t = \frac{-P}{2\pi(1/\alpha^2-1)} \left\{ (1+\nu_r) - \frac{1+\nu_t}{\alpha} \left(\frac{r}{R}\right)^{\alpha-1} \right\}$$

$$M_r = \frac{-P(1+\nu_t)}{2\pi(1-\alpha^2)} \left\{ +1 - \left(\frac{r}{R}\right)^{\alpha-1} \right\}$$

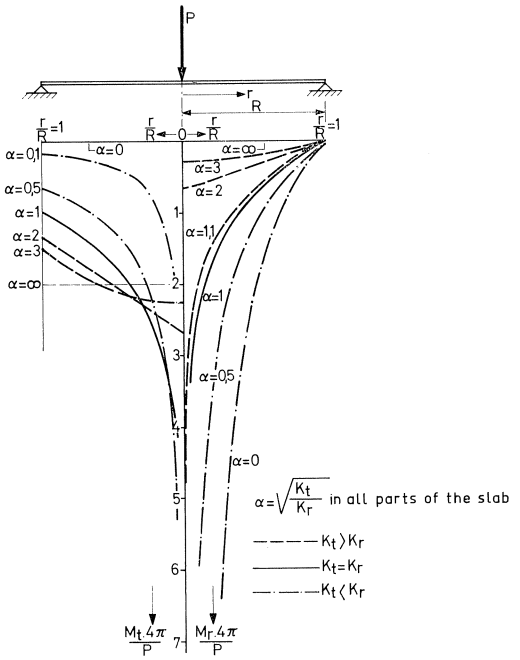

Fig. 15. Distribution of radial and tangential bending moments.

From this diagram it emerges that for values of $\alpha > 1$ (i.e., if the tangential flexural rigidity is greater than the radial flexural rigidity) the bending moment distribution in the slab no longer shows a singularity. The moments at the centre of the slab now are of finite magnitude. For $\alpha = 2$ (i.e., if the tangential flexural rigidity is four times the radial flexural rigidity) a substantial reduction of the extreme moments has occurred and the distribution of the moment across the slab is much more uniform.

For values of $\alpha < 1$ the distribution of the tangential moments becomes even more unequal than for $\alpha = 1$ and the radial moments increase considerably in magnitude. Values of $\alpha < 1$ appear to have an unfavourable effect.

In reality the loaded reinforced concrete slab has zones with different flexural rigidities because of the progressive cracking of the concrete (in two directions) and the yielding of the reinforcement. The considerations presented above were intended merely to serve an illustrative purpose.

Collapse behaviour (point load)

From Fig. 10 it is apparent that, besides, the rigidity of the slab, its strength is also to a great extent determined by the quantity of tangential reinforcement. The shape of the curves in that diagram suggests that collapse of the slabs 11, 12 and 14 occurred rather suddenly. In the case of slabs 13A, 13B and 15 it was found that, with the approach of collapse, the deflection increased greatly, which indicates gradual collapse. An inspection of the collapsed slabs (Figs. 16 to 21) shows that collapse of the slabs can occur before the radial cracks in which yielding of the steel develops have reached the bearings and that in the state of collapse one or more circular cracks may occur on the loaded side of the slab. In every case a conical portion was forced out of the slab at the point load.

The slabs 13A and 13B (Figs. 18 and 19) display on the tensile side a very dense pattern of radial cracks extending to the bearings. There are circular cracks on the loaded side of these slabs. In slabs 11 and 14 (Figs. 16 and 20) collapse occurred before the radial cracks had reached the bearings. In slab 14 an incipient circular crack on the loaded side of the slab can be seen.

Slab 12 (Fig. 17) is very similar to slab 11, except that some of the radial cracks have reached the bearings.

Slab 15 (Fig. 21), provided with orthogonal mesh reinforcement for the purpose of comparison, in the collapsed state has a not fully developed radial cracking pattern (as slabs 11, 12 and 14 have) and displays a circular crack on the loaded side (cf. 13A and 13B). A conical portion has been forced quite out of the slab at the centre. The three holes around it served for measuring the concrete cover and the thickness of the slab.

With regard to the magnitude of the collapse load (ultimate load P_u) an attempt can be made to predict this on the basis of the collapse mechanism which K. W. Johansen has indicated for circular isotropic slabs (Fig. 22) and which is also adopted in CUR Report 26A, ref. [2].

From a consideration of the equilibrium of a slab segment it follows that:

$$P_{u,1} = 2 \cdot \pi \cdot M_{t,p}$$

Comparison of the collapse loads calculated in the above manner with the experimentally obtained values (Fig. 23) shows that great differences are liable to occur.

The slabs 11, 12 and 14 collapsed before $P_{u,1}$ was attained. The collapse loads of the slabs 13A, 13B and 15 were substantially higher than calculated according to Johansen.

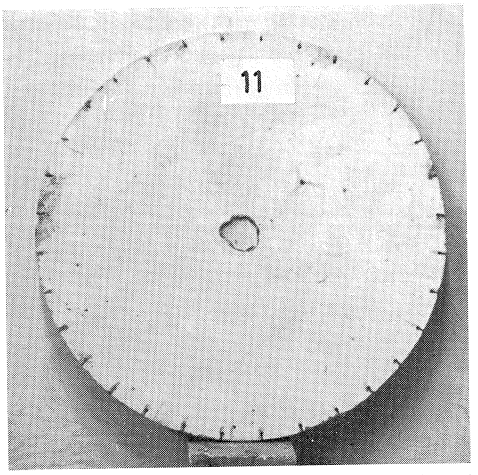

loaded side

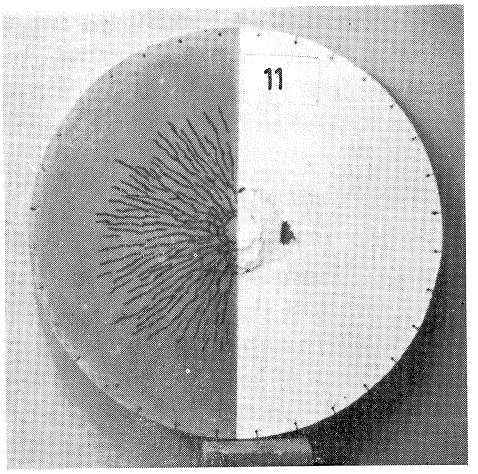

top

Fig. 16. Slab 11.

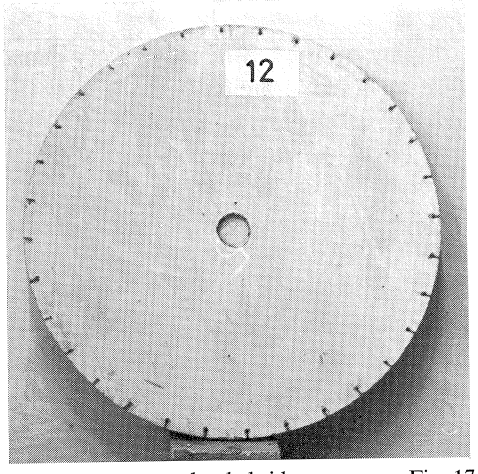

loaded side

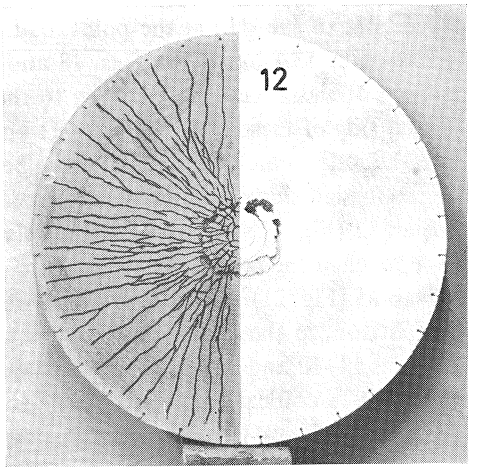

top

Fig. 17. Slab 12.

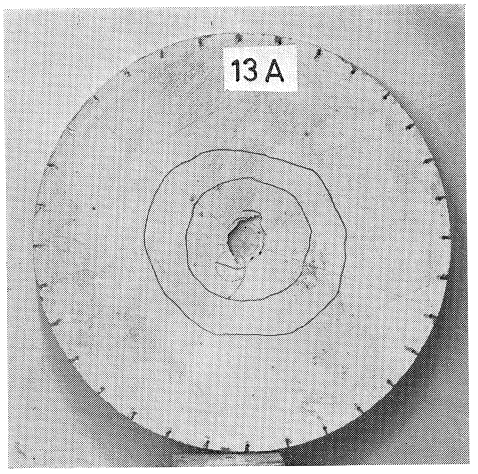

loaded side

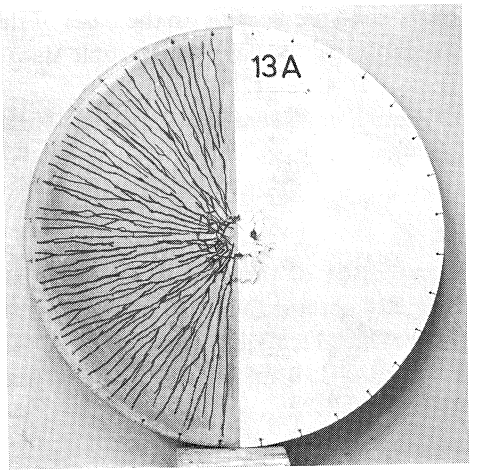

top

Fig. 18. Slab 13a.

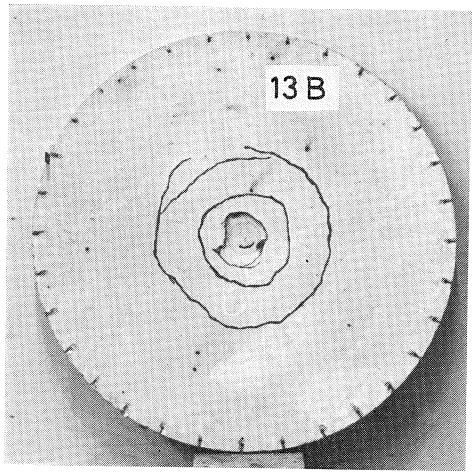

loaded side

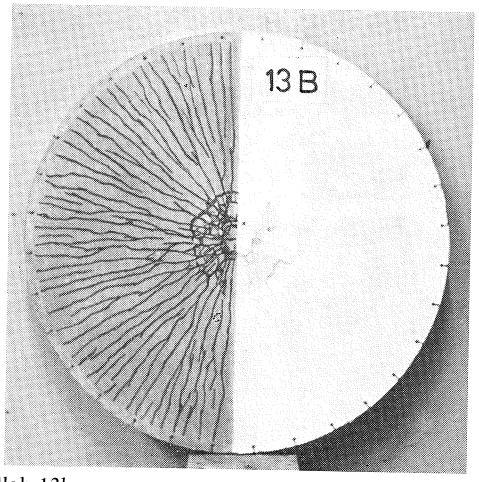

top

Fig. 19. Slab 13b.

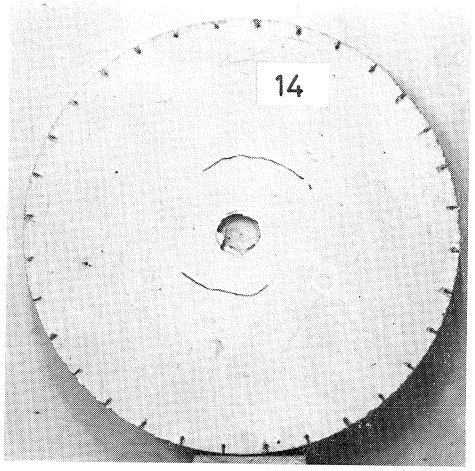

loaded side

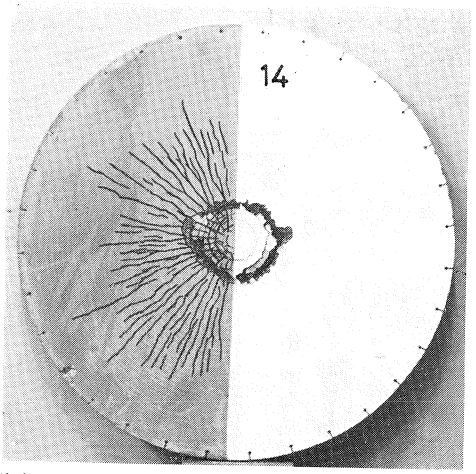

top

Fig. 20. Slab 14.

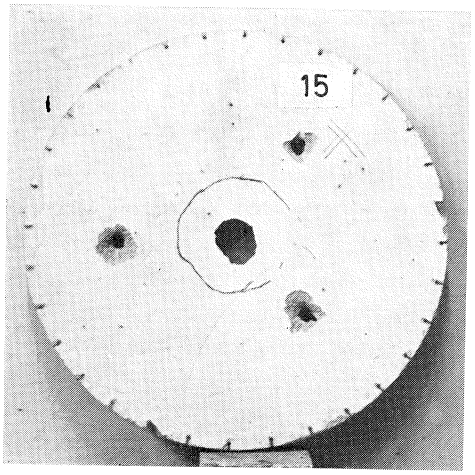

loaded side

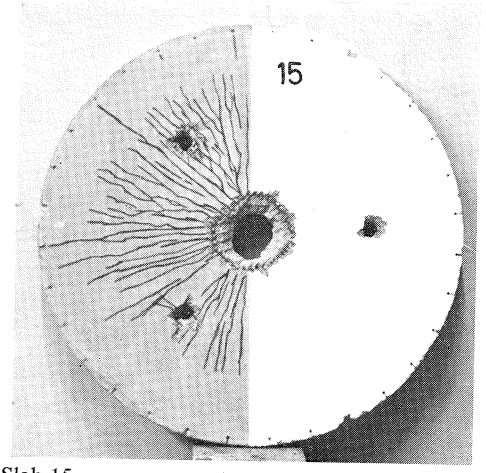

top

Fig. 21. Slab 15.

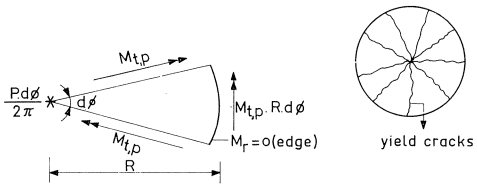

Fig. 22. Equilibrium of a slab segment at collapse, according to Johansen (point load).

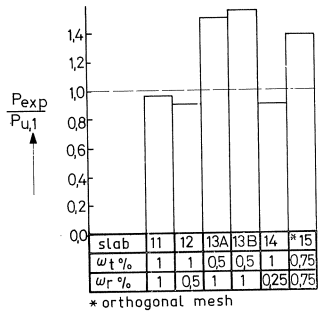

Fig. 23A. Comparison of P_{exp} with $P_{u,1}$.

slab	Pexp	Pu,1	Pu,2
11	15,2	15,8	20,1
12	14,5	16,1	20,4
13 A	10,5	7,0	11,1
13 B	10,8	6,9	11,1
14	14,0	15,5	19,5
15	12,7	9,3	13,6

Fig. 23B. Experimentally determined and calculated collapse loads in kN.

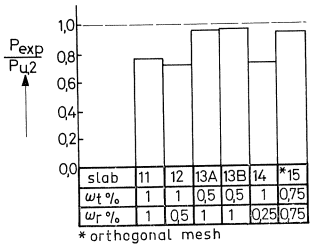

Fig. 23C. Comparison of P_{exp} with $P_{u,2}$.

Collapse load calculated according to Johansen not reached in the slabs 11, 12 and 14

It has already been mentioned that when these slabs collapsed the radial yield cracks had not yet fully developed, although the magnitude of the load had come fairly close to the collapse load calculated in accordance with Johansen's method. This last-mentioned phenomenon indicates the development of a compression ring in the outermost part of the slab. This will be further considered later on. Suffice it to mention here that, as a result of this behaviour, the collaps load associated with the mechanism already referred to could well have been considerably greater than the collapse load according to Johansen, but that some other phenomenon intervened to prevent this.

The fairly sudden collapse that occurred in these slabs is a further indication in that direction. Collapse may have been caused by the rotational capacity having been exceeded at sections under and beside the point load, where very large curvatures occur, and by the phenomenon of punching shear. As regards the latter it can be pointed out that, in consequence of bending, the tensile zone of the concrete was rendered incapable of co-operating and that therefore the large shear stresses had to be transmitted by the compressive zone only. It will not, however, be attempted here to enter into a discussion of this complex phenomenon.

Collapse load calculated according to Johansen exceeded in the slabs 13A, 13B and 15

To explain why the collapse load $P_{u,1}$ was exceeded it is necessary to include the membrane forces, which develop with increasing deflection of the slab, in the consideration of the problem. A "compression ring" will be formed in the outer part of the slab, as a result of which the moment M_t that can be resisted in the tangential direction can substantially increase in magnitude.

Fig. 44 shows how the moment that can be resisted at a section varies when a normal compressive force is transmitted across the section. In the accompanying table the ratio of the maximum moment that can be resisted $M_{\max}$ and the plastic moment M_p is given for the various reinforcement percentages employed in the slabs. The propagation of the radial yield cracks from the centre of the slab will be halted when these cracks reach the compression ring. As a result of this a collapse mechanism is found to occur in which tangential tensile cracks develop on the loaded side of the slab (Figs. 18, 19, 21 and 24).

The magnitude of the collapse load can be determined from considerations of equilibrium (Fig. 25).

Since the reinforcement percentage ω_t is less than ω_r in the slabs considered here

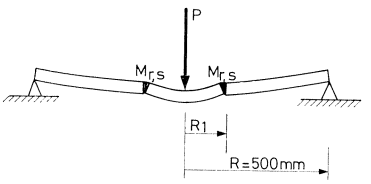

Fig. 24. Collapse mechanism of a slab under point load (slabs 13A, 13B and 15).

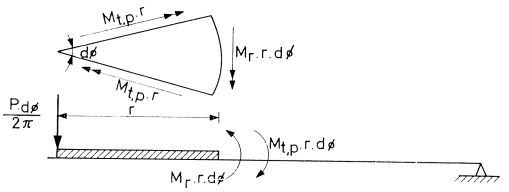

Fig. 25. Equilibrium of a slab segment where $M_{t,p}$ has been reached in the tangential direction.

(13A, 13B and 15), yielding will occur first in the tangential reinforcement. In Fig. 25 it is indicated that the tangential moment M_t has attained the value $M_{t,p}$ (the plastic moment in that direction) over a distance r from the centre of the slab. From the equilibrium of the slab segment it follows that:

$$P/2\pi = M_{t,p} - M_r$$

If $M_t = M_{t,p}$ the load P can further increase if M_r decreases.

It follows from the above that there is no point in providing the slab with more reinforcement in the radial direction than in the tangential direction.

For $M_r = 0$ the value found for the load P is precisely $P_{u,1}$ (Johansen); in this case M_r is therefore zero in every part of the slab. If M_r can moreover take on negative values, then P can become even larger.

If there is no top reinforcement, the largest value of P is attained when M_r becomes equal to the cracking moment $M_{r,s}$ of the section. With $M_r = -M_{r,s}$ the following expression is then obtained for the collapse load $P_{u,2}$:

$$P_{u,2}/2\pi = M_{t,p} + M_{r,s}$$

As a result of an increase in the magnitude of the tangential moment M_t that can be resisted in the outer part of the slab – in this case because of the development of a compression ring – the collapse load $P_{u,2}$ is larger than $P_{u,1}$.

$M_{r,s}$ can be determined with the data given in Appendix A. $P_{u,2}$ provides a good approximation of the observed collapse load for the slabs 13A, 13B and 15, as appears from Fig. 23.

That the actual collapse load is somewhat less than $P_{u,2}$ may be due to the fact that the moments $M_{t,p}$ in the central part of the slab are reduced a little by tensile membrane forces and to a reduction of the flexural strenght of the concrete in consequence of the biaxial state of stress.

Because of the increase in the tangential moment M_t that can be resisted in the outer part of the slab (the compression ring) the collapse load of this part is greater than $P_{u,2}$, so that the collapse of the inner part of the slab is the determining factor.

Summary (see Fig. 23)

In this part of the research (point load) two forms of collapse manifested themselves.

The slabs 13A, 13B and 15, which were of relatively low rigidity because of the small quantity of tangential reinforcement and in which, with increasing deflection, a compression ring was able to develop in the outer part, collapsed in accordance with the mechanism as discussed here at a load $P_{u,2}$ which exceeded the collapse load $P_{u,1}$ according to Johansen's elementary theory. The collapse load $P_{u,2}$ was then in part dependent on the magnitude of the cracking moment of the concrete. The development of a compression ring was made possible by the "free" support conditions of the slab (Fig. 5).

The more rigid slabs 11, 12 and 14 (with a higher percentage of tangential reinforcement) collapsed rather suddenly at a load which was a little below the collapse load value calculated according to the elementary theory, which is probably due to the rotational capacity of the sections being exceeded and to the phenomenon of punching shear.

3.3 *Slabs loaded by a uniformly distributed load*

On comparing the slabs 01, 02, and 03 (Fig. 11) it appears that the effect of the percentage of radial reinforcement on the behaviour of the slab is somewhat greater than in the case of slabs loaded by a point load.

However, on comparing the behaviour of a slab in which ω_r is reduced by half (slab 01 → slab 02) with that of a slab in which ω_t is reduced by half (slab 01 → slab 04), it is found that also in the case of uniformly distributed load the tangential flexural rigidity of the slab is of considerably more influence on its rigidity and strength than the radial flexural rigidity is.

In this case, too, it was investigated with the aid of the theory for the cylindrical orthotropic slab what effect α $(=\sqrt{k_t/k_r})$ has upon the deflections and bending moments.

The deflection at the centre of the slab for three values of α is indicated in Fig. 26.

UNIFORMLY DISTRIBUTED LOAD

flexural rigidities	$\alpha=\sqrt{K_t/K_r}$	deflection at centre of slab (W)	W in %
$K_r=2K$ $K_t=2K$	1	$0.039\frac{qR^4}{K}$	100
$K_r=K$ $K_t=2K$	$\sqrt{2}$	$0.045\frac{qR^4}{K}$	115
$K_r=2K$ $K_t=K$	$\frac{1}{2}\sqrt{2}$	$0.066\frac{qR^4}{K}$	169

Fig. 26. Theoretical effect of k_t and k_r on deflection at the centre of the slab.

From this it appears that with uniformly distributed load a reduction of the radial flexural rigidity by half has a somewhat greater effect on the deflection at the centre of the slab than in the case of the point load. On the other hand, halving the tangential rigidity again has much greater effect. Both these results are in agreement with the experimental evidence.

The radial and tangential bending moments for various values of α are given in Fig. 27. From this diagram it emerges that for values of $\alpha > 1$ (i.e., if the tangential flexural rigidity exceeds the radial flexural rigidity) the moments at the centre decrease in magnitude.

The highest values now occur in a zone situated further outwards.

For *values of* α *less than unity* ($\alpha < 1$) a singularity occurs at the centre of the slab. The moments become infinitely large at that point. More particularly the radial moments in the slab increase considerably. Values of α less than unity thus again apparently have an unfavourable effect.

An *analysis* with the aid of the finite element method (using annular elements, Fig. 28) – taking account of gradual progressive cracking of the concrete and the slab rigidities thereafter determined by the reinforcement percentages, but not taking account of the yielding of the reinforcement and the membrane forces that occur – results for the slabs 02 and 04 in bending moment diagrams as indicated in Figs. 29 and 30, which still show a distinct similarity with the diagrams in Fig. 27.

As a result of yielding of the radial and/or tangential reinforcement a redistribution of moments will occur in reality, which will be further considered later on.

From Fig. 30 it also appears that a value of α less than unity is unfavourable with regard to the bending moment distribution, resulting in diminished rigidity of the slab (Fig. 11).

With the aid of the above-mentioned analysis it is also possible to determine the load-deflection diagrams of the slabs for point load as well as for uniformly distributed load. An example is given in Fig. 31.

$$M_r = \frac{-q.R^2(3+\nu_t)}{(18-2\alpha^2)} \left\{ \left(\frac{r}{R}\right)^2 - \left(\frac{r}{R}\right)^{\alpha-1} \right\}$$

$$M_t = \frac{-q.R^2}{(18/\alpha^2-2)} \left\{ \left(\frac{r}{R}\right)^2 (1+3\nu_r) - \frac{3+\nu_t}{\alpha} \left(\frac{r}{R}\right)^{\alpha-1} \right\}$$

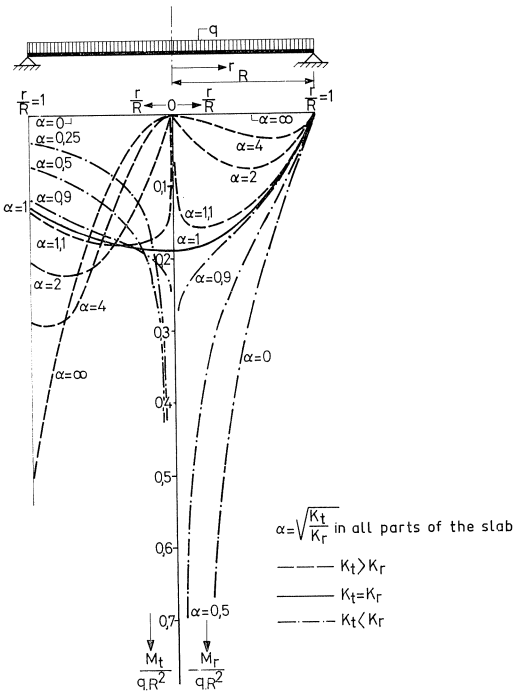

Fig. 27. Distribution of radial and tangential bending moments.

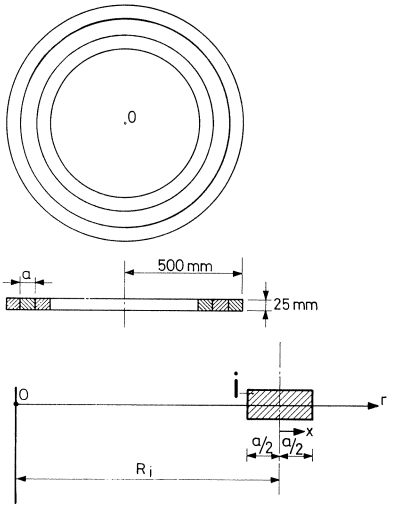

Fig. 28. Annular slab elements, used in the analysis of the slabs tested.

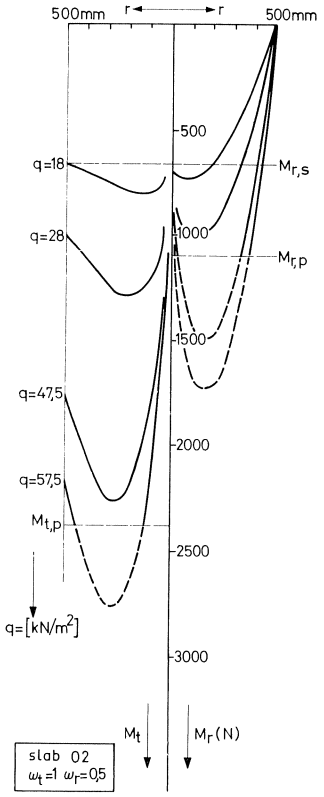

Fig. 29.

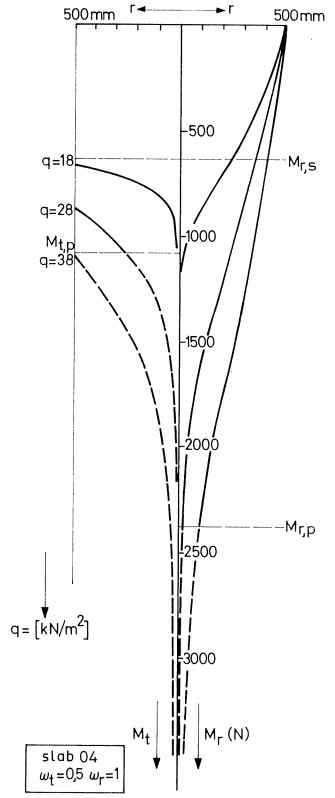

Fig. 30.

Distribution of the radial and tangential moments in the slabs 02 and 04 under increasing loads.

Under working load conditions, i.e., for deflections up to about 4 mm, the analysis provides a good approximation of the actual behaviour of the slabs. Since the effect of yielding of the reinforcement has not been allowed for in these calculations, however, for larger values of the deflection the difference between the results of the analysis and those obtained in the model becomes greater.

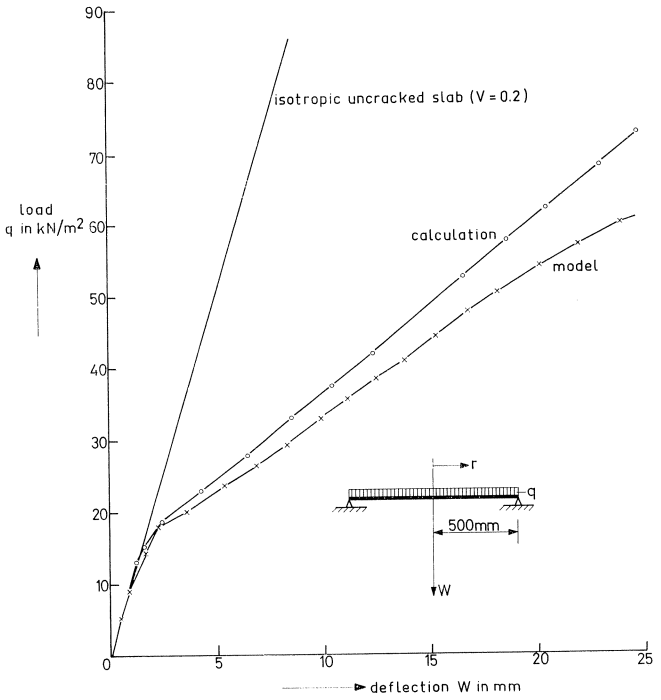

Fig. 31. Load-deflection diagram of slab 01 as obtained experimentally and by calculation.

Collapse behaviour (uniformly distributed load)

In this form of loading applied to the slab the tangential reinforcement likewise has a greater effect on the rigidity and strength of the slab than the radial reinforcement has. In comparison with point load, however, the effect of the radial reinforcement on the collapse load in the present case is more pronounced. In the calculation of this collapse load the magnitude of the yield moment in the radial direction ($M_{r,p}$) will, as contrasted with the case of point load on the slab, therefore also play a part.

The slabs 02 and 03 (Figs. 33 and 36 to 39) and, to a less extent, slab 01 (Fig. 32) exhibit a wide circular crack on the tensile side on the state of collapse; this crack goes right through the slab to the compressive side. In the outer part of these slabs there are radial cracks extending to the bearings.

From the moiré pattern in the state of collapse of the slabs 02 and 03 (Figs. 8 and 9)

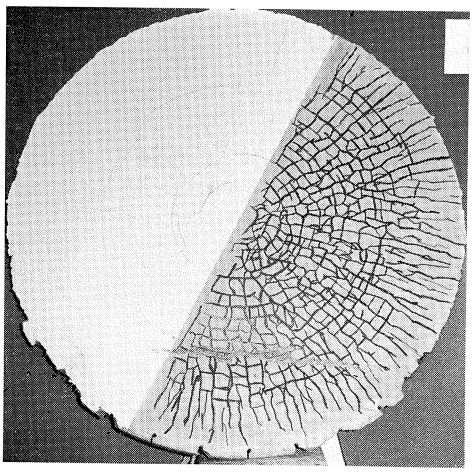

Fig. 32. Slab 01 (tensile side).

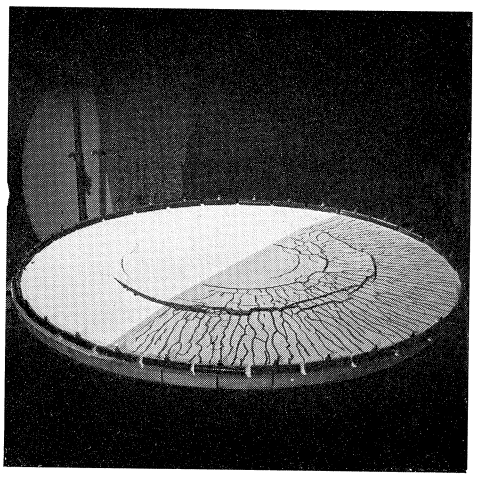

Fig. 33. Slab 03 (collapse pattern).

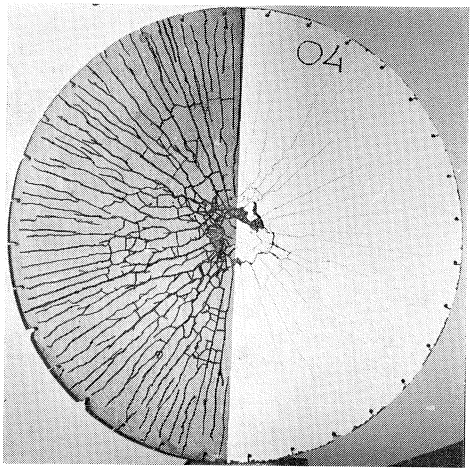

Fig. 34. Slab 04 (tensile side).

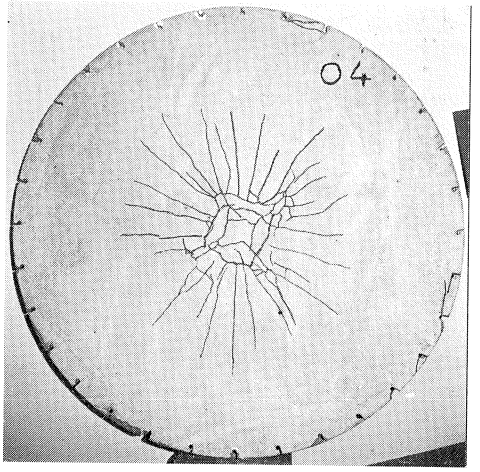

Fig. 35. Slab 04 (compressive side).

it is apparent that the inner part of the slab is almost plane, while the outer part is conical.

Slab 04 (Figs. 34 and 35) undergoes conical collapse and is seen to have radial cracks also on the compressive side.

For the slabs with uniformly distributed load a comparison has, to begin with, again been made between the experimentally determined collapse loads and those calculated according to Johansen (Fig. 40).

The starting point of the analysis based on Johansen's approach is the same yield line pattern as that associated with the point load (Fig. 22). In this case we obtain from considerations of equilibrium:

$$q_{u,1} = 6M_{t,p}/R^2$$

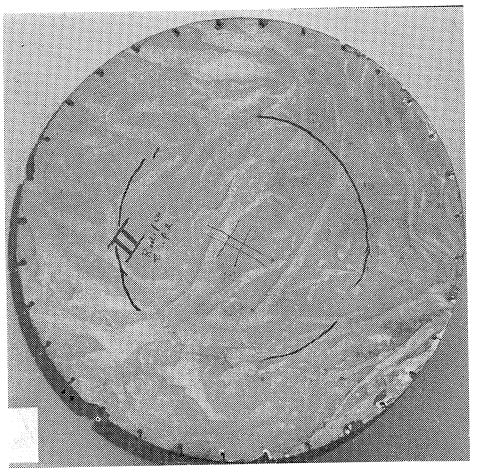

Fig. 36. Slab 02 (compressive side).

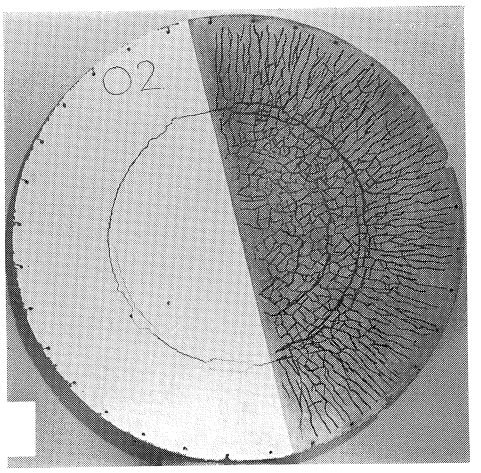

Fig. 37. Slab 02 (tensile side).

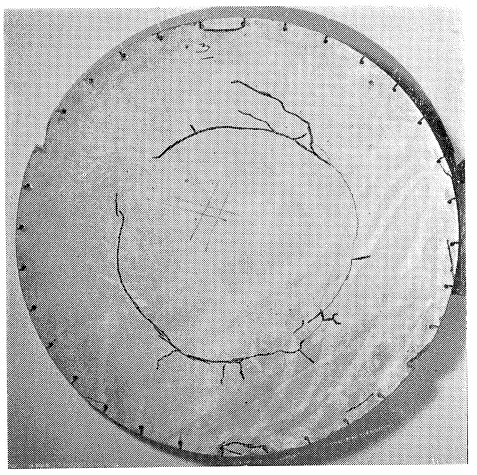

Fig. 38. Slab 03 (compressive side).

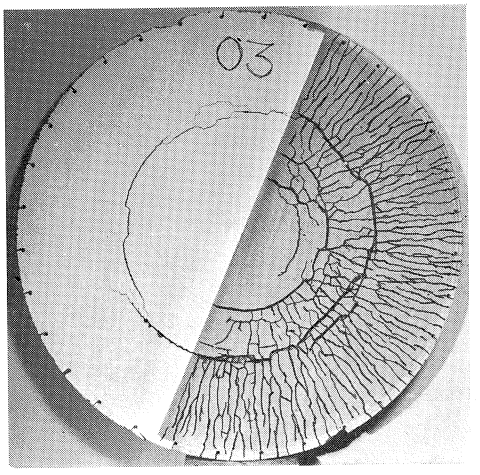

Fig. 39. Slab 03 (tensile side).

It appears that slab 03 collapses before $q_{u,1}$ is attained, whereas in the case of the other slabs $q_{u,1}$ is exceeded. For slab 04 the collapse load is indeed equal to twice $q_{u,1}$.

The observed collapse mechanism does not, however, correspond to that of Fig. 22. For the slabs 01, 02 and 03 the collapse mechanism is shown again in Fig. 41.

This mechanism comprises a fairly flat central portion and a conically shaped outer region (Figs. 8 and 9). It is due to the fact that the largest radial bending moment does not occur at the centre of the slab (Figs. 27 and 29), but approximately at the tangential cracks which penetrate through the slab to the compressive side thereof (Figs. 36 to 39). Since the central region of the slab remains almost plane, the collapse of the outer part of the slab will be of deciding importance with regard to the magnitude

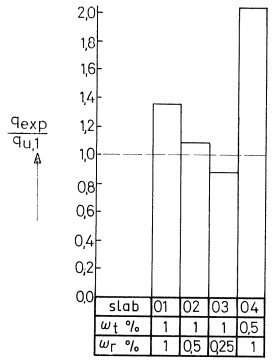

Fig. 40A. Comparison of q_{exp} with $q_{u,1}$.

slab	R1exp	R1	q_{exp}	$q_{u,1}$	$q_{u,2}$	$q_{u,3}$	$q_{u,4}$
	cm		kN/m^2				
01	–	9,15	79	58	57	79	–
02	28	23,2	63	58	48	63	–
03	28	28,8	50	57	36	49	–
04	–	0	53	26	26	70	53

Fig. 40B. Maximum load q (kN/m^2) and position of the tangential crack (cm) as determined experimentally and by calculation.

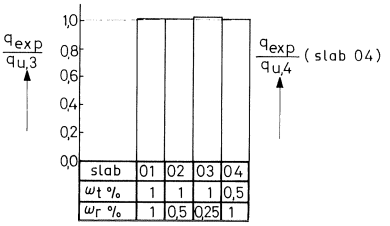

Fig. 40C. Comparison of q_{exp} with $q_{u,3}$ and $q_{u,4}$ respectively.

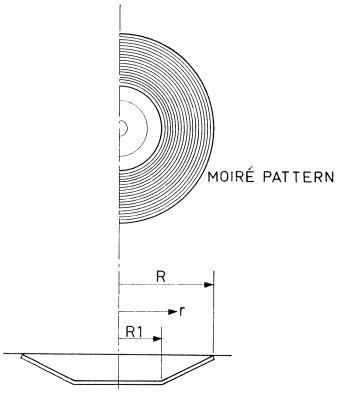

Fig. 41. Collapse mechanism of the slabs 01, 02 and 03.

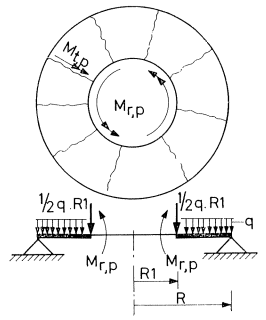

Fig. 42. Collapse mechanism of the slabs 01, 02 and 03.

of the collapse load. Fig. 42 shows this part of the slab with the forces that act on it.

The magnitude of the collapse load $q_{u,2}$ follows from the equilibrium of the annular part of the slab:

$$q_{u,2} = \frac{M_{r,p} \cdot R_1 + M_{t,p}(R - R_1)}{\frac{1}{6}(R^3 - R_1^3)} \tag{1}$$

The position of the tangential crack – which is given by R_1 – remains to be determined.

In Fig. 43 the collapse load $q_{u,2}$ has been plotted as a function of R_1.

The least value of q determines the position of the tangential crack. This can therefore be determined by differentiating q with respect to R_1 and equating the resulting expression to zero; $M_{r,p}$ and $M_{t,p}$ are assumed independently of R_1.

With $dq/dR_1 = 0$ we obtain:

$$2M_{r,p} \cdot R_1^3 - 2M_{t,p} \cdot R_1^3 + 3M_{t,p} \cdot R \cdot R_1^2 + M_{r,p} \cdot R^3 - M_{t,p} \cdot R^3 = 0$$

The values obtained for R_1 for the slabs 01, 02 and 03 from this equation are presented in Fig. 40B.*) For 02 and 03 they are in reasonably good agreement with the experi-

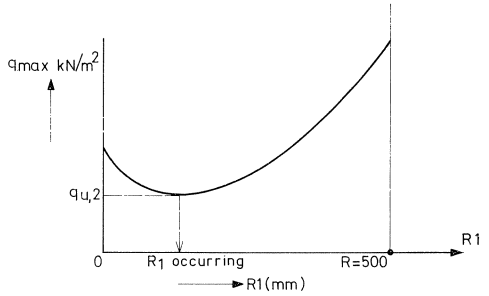

Fig. 43. Maximum load (q_{max}) as a function of the position of the tangential crack (R_1) (slabs 01, 02 and 03).

*) Since the radial yield moment $M_{r,p}$ for slab 03 is smaller than the cracking moment $M_{r,s}$, this latter moment has been substituted for $M_{r,p}$ in calculating R_1 for this slab.

mentally determined values. For slab 04 there is no mathematical minimum. In this case the lowest value of q occurs at $R_1 = 0$, which corresponds to the conical surface found to develop in slab 04 (Fig. 34) and to the fact that the maximum radial moment in this slab occurs at the centre thereof (Figs. 27 and 30).

With the values obtained for R_1 the collapse loads $q_{u,2}$ can now be calculated from the formula (1). They are found to differ considerably from the experimentally determined values (Fig. 40).

For the slabs for which $M_{r,p}$ is smaller than $M_{t,p}$ the values thus obtained are even *lower* than $q_{u,1}$. This will readily be understood on considering again the equilibrium of a sector of the annular part in Fig. 42. Hence we here have the case where anisotropy ($\omega_r < \omega_t$) results in a different collapse mechanism with a lower collapse load than in the isotropic case. This means that there is no point in making ω_r less than ω_t.

That the slabs do not collapse under the load $q_{u,2}$ is due to the fact that with this manner of loading, too, the moment that can be resisted in the tangential direction (M_t) is increased by the effect of membrane forces (Fig. 44).

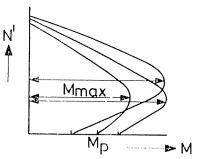

slab	ω_t %	$M_{t,max}/M_{t,p}$
01	1,127	1,45
02	1,136	1,45
03	1,157	1,44
04	0,606	2,67
11	1,078	1,48
12	1,067	1,48
13A	0,588	2,70
13B	0,557	2,84
14	1,102	1,46
15	ω_l 0,688	2,18

Fig. 44. Relationship between N' and M and the ratio between $M_{t,max}$ and $M_{t,p}$.

On replacing $M_{t,p}$ in formula (1) by $M_{t_{max}}$ – the calculation of which is given in Appendix A – we obtain:

$$q_{u,3} = \frac{M_{r,p} \cdot R_1 + M_{t_{max}}(R - R_1)}{\frac{1}{6}(R^3 - R_1^3)} \tag{2}$$

The values of $q_{u,3}$ calculated in this way are listed in the table in Fig. 40. For the slabs 01, 02 and 03 they are found to be in very good agreement with the experimentally determined values. The percentage increase of $q_{u,3}$ in relation to $q_{u,2}$ is very nearly the same for the three slabs ($\sim 35\%$).

If the collapse load of slab 04 is calculated in the same way, the value obtained is too high. The reason for this is that in the above consideration of the problem $M_{t_{max}}$ is assumed to be constant across the width of the outer ring (the conical surface). If this part extends to the centre of the slab, however, this assumption is not permissible. M_t will decrease progressively from the edge to the centre of the slab. On the assumption that at the edge of the slab $M_t = M_{t_{max}}$ and at the centre $M_t = M_r = M_{t,p}$

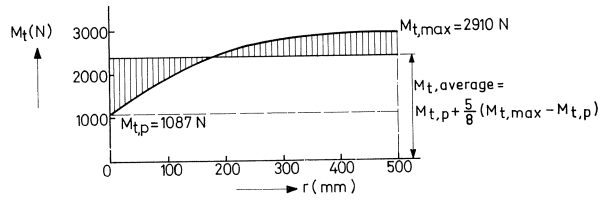

Fig. 45. Parabolic distribution of the tangential moment in slab 04.

and that there is a parabolic distribution between these values (Fig. 45), the following expression is obtained for the collapse load:

$$q_{u,4} = \frac{M_{t,p} + \frac{5}{8}(M_{t_{max}} - M_{t,p})}{\frac{1}{6} \cdot R^2}$$

The value $q_{u,4}$ thus calculated for slab 04, likewise included in the table in Fig. 40, is found to be in good agreement with the experimentally determined value. The assumption of a parabolic distribution across the slab corresponds suitably to a linear distribution of the tangential normal forces such as occur on deformation of the slab to a conical surface and to the relation between normal force and the moment that can be resisted (Fig. 44).

Summary (see Fig. 40)

From this part of the research it therefore emerges that differences in the reinforcement percentages in the tangential and the radial direction can result in a considerable change in the bending moment distribution after cracking. This may give rise to a collapse mechanism which differs from that envisaged by Johansen's elementary theory for the isotropic slab and which may result in *lower* collapse loads.

The membrane action (compression ring), which has the effect of increasing the moment that can be resisted in the tangential direction, is the reason why higher values may nevertheless be found for the collapse load.

4 Conclusions

If cracking of the concrete results in a condition in which the flexural rigidity in the radial direction of the slab differs from that in the tangential direction because the reinforcement percentages in these directions are different, this may greatly affect the deflection of the slab. It was found that, for equal quantities of reinforcement per unit area, the deflection of one slab could be twice as large as that of another. The deflection was found to be determined more particularly by the tangential reinforcement.

The differences in flexural rigidity may also result in a totally different bending moment distribution as compared with the isotropic slab, so that very different col-

lapse mechanisms may ensue. In the case of uniformly distributed load, for example, it was found in those instances where the radial reinforcement percentage was smaller than the tangential reinforcement percentage that the deflection surface was not a conical surface with radial cracks across the entire diameter, but was a truncated cone. The central part of the slab remained substantially plane, and a circumferential yield crack developed at the transition to the conical part.

The collapse load associated with this collapse mechanism was lower than that for the isotropic slab with the same amount of tangential reinforcement. The position of the yield crack in the circumferential direction depends on the ratio of the tangential and radial reinforcement percentages.

Although increasing the tangential reinforcement percentage has a favourable effect on the rigidity of the slab, it should be borne in mind that it is not attended by a proportional increase in the collapse load, since this trend is affected by the development of a different collapse mechanism.

Membrane forces may develop with increasing magnitude of the deflection, while a compression ring is formed in the outer part of the slab. As a result of the internal compressive forces the tangential moments that can be resisted in this zone may be considerably greater than the full plastic moment. This is the reason why, in the case of uniformly distributed load, the collapse loads were found to be considerably higher than those obtained by calculation with full plastic moments. A simple procedure for calculating this increase in collapse load was established.

In the case of the slab subject to point load it was found that the development of a compression ring could give rise to a different collapse mechanism, in connection with which a crack in the circumferential direction was formed on the loaded side of the slab in consequence of the tensile strength of the concrete being exceeded. The resulting increase in the collapse load depended on the magnitude of the negative radial cracking moment and was therefore not difficult to determine.

In the tests with point loads it was also found that collapse loads might occur lower than the values calculated according to the elementary collapse analysis for an isotropic slab with the same amount of tangential reinforcement. The phenomenon of punching shear played a part here, this being promoted by the very large curvatures which occur at the centre of the slab and which probably also caused the rotational capacity to be exceeded.

Concluding remarks

The results of the research reported here give rise to some inferences of more general scope:

1. Deviation of the reinforcement pattern from isotropy may result in substantially different deflections (see Figs. 10 and 11, for example).
2. It may also result in collapse mechanisms which are difficult to ascertain, which are initiated by deviant bending moment distributions, and which may result in

lower collapse loads than in the case of isotropic slabs with the same amount of tangential reinforcement.

3. Concentrated loads may give rise to sudden failure at a load which is smaller than the collapse load according to the yield-line theory.
4. In some cases it is possible to assess the favourable effect of membrane action in a simple way, without second-order analysis.

References

1. CARRIER: Stress distribution in cylindrically aeolotropic plates. Journal of Applied Mechanics, 1943, Vol. 10, No. 3 and 1944. Vol. 11, No. 3.
2. CUR Report 26A: De berekening van platen volgens de vloeilijnentheorie (The analysis of slabs according to the yield-line theory). Netherlands Committee for Concrete Research, Zoetermeer.
3. CUR Report 65: Pons (Punching shear). Netherlands Committee for Concrete Research, Zoetermeer.

Appendix A: Data of the slabs

point load

slab	h_{tot}	h_t	h_r	ϕ_t	ϕ_r	d_t	d_r	$\sigma_{ae,t}$	$E_{a,t}$	$\sigma_{ae,r}$	$E_{a,r}$
11	26,1	23,0	21,1	1,99	1,99	3,02	5,0	0,476	199,3	0,476	199,3
12	26,2	23,3	21,62	1,99	1,385	2,89	4,58	0,476	199,3	0,472	200,0
13A	25,6	20,4	22,25	1,385	1,99	5,13	3,45	0,472	200,0	0,476	199,3
13B	26,0	21,6	23,32	1,385	1,99	4,36	2,68	0,438	188,0	0,476	199,3
14	25,5	22,5	21,12	1,99	1,01	2,92	4,42	0,476	199,3	0,281	199,3
15	26,1	21,95	21,95	1,55 ϕ_x	1,55 ϕ_y	4,15 *)	4,15 *)	0,469	199,3	0,469	199,3
			mm						kN/mm²		

*) mean value for dx and dy

uniformly distributed load

slab	h_{tot}	h_t	h_r	ϕ_t	ϕ_r	d_t	d_r	$\sigma_{ae,t}$	$E_{a,t}$	$\sigma_{ae,r}$	$\mathbf{E}_{a,r}$
01	25,6	22,1	20,08	1,99	1,99	3,53	5,52	0,476	199,3	0,476	199,3
02	25,63	21,9	20,23	1,99	1,385	3,72	5,40	0,476	199,3	0,472	200,0
03	25,49	21,6	20,01	1,99	1,01	3,91	5,40	0,476	199,3	0,281	199,3
04	25,2	19,9	21,57	1,385	1,99	5,31	3,63	0,472	200,0	0,476	199,3
			mm						kN/mm²		

point load

slab	ω_t %	ω_r %	$M_{t,p}$	$M_{r,p}$	$M_{r,s}$	$M_{t,\max}$	P_{exp}	$P_{u,1}$	$P_{u,2}$	$P_{u,\text{punching shear}}$
11	1,078	1,179	2518	2301	681	3720	15,2	15,8	20,1	15,2
12	1,067	0,557	2560	1183	686	3785	14,5	16,1	20,4	15,2
13A	0,588	1,123	1110	2448	655	2003	10,5	7,0	11,1	14,8
13B	0,557	1,067	1099	2565	676	3124	10,8	6,9	11,1	15,1
14	1,102	0,304	2460	377	650	3582	14,0	15,5	19,5	14,8
15	0,688*)	0,688*)	1477	1484	681	3215	12,7	9,3	13,6	15,2
			N				kN			

*) ωx and ωy

$M_{r,s}$: negatieve bending moment; reinforcement neglected

$\sigma_b = 6$ N/mm²

$$P_{u,1} = 2 \cdot \pi \cdot M_{t,p}$$

$$P_{u,2} = 2 \cdot \pi \cdot (M_{t,p} + M_{r,s})$$

$$P_{u_{\text{punching shear}}} = \pi \cdot \left(75 + \frac{h_{tot}}{2}\right) \cdot \frac{h_{tot}}{2} \cdot \sigma_{sp}$$

uniformly distributed load

slab	ω_t %	ω_r %	$M_{t,p}$	$M_{r,p}$	$M_{r,s}$	$M_{t,\max}$	q_{exp}	$q_{u,1}$	$q_{u,2}$	$q_{u,3}$	$q_{u,4}$
01	1,127	1,239	2422	2181	–	3520	79	58	57	79	–
02	1,136	0,596	2396	1106	–	3490	63	58	48	63	–
03	1,157	0,32	2370	355	661	3420	50	57	36	49	–
04	0,606	1,1535	1087	2357	–	2910	53	26	26	70	53
			←			N	→	←		kN/m²	→

slab	$R_{1,exp}$	R_1
01	–	91,5
02	280	232
03	280	288
04	–	0
	(mm)	(mm)

$$q_{u,1} = \frac{6 \cdot M_{t,p}}{R^2}$$

$$q_{u,2} = \frac{M_{r,p} \cdot R_1 + M_{t,p}(R - R_1)}{\frac{1}{6}(R^3 - R_1^3)}$$

$$q_{u,3} = \frac{M_{r,p} \cdot R_1 + M_{t_{max}}(R - R_1)}{\frac{1}{6}(R^3 - R_1^3)}$$

$$q_{u,4} = \frac{6 \cdot M_{t,p} + \frac{5}{8}(M_{t_{max}} - M_{t,p})}{R^2}$$

The effect of normal (compressive) stresses on the moment that can be resisted

If no resultant normal force is acting on a section, the magnitude of the *yield moment* in the radial or the tangential direction can be deduced from considerations of equilibrium.

The plastic moment per unit length is:

$$M_p = \omega \cdot h \cdot \sigma_{ae}(h - \tfrac{3}{8}x) \qquad \text{(N)}$$

Note: x = depth of concrete compressive zone
σ'_{bu} = 0.8 × average cube strength

For the various slabs this moment had been calculated both in the radial ($M_{r,p}$) and in the tangential direction ($M_{t,p}$) (see page 31 and 32).

In consequence of compressive stresses on the section the moment to be transmitted will be increased. In general, the relationship between a normal force and the moment that can be resisted will be as shown in Fig. 44, where this relationship has been plotted for a few cases.

In cases where higher reinforcement percentages (ω = approx. 1%) were provided there also occurred yielding of the reinforcement at M_{max}. With lower percentages (ω = approx. 0.5%) there was no yielding of the reinforcement at M_{max}.

For the calculation of M_{max} it is necessary to base oneself on the maximum compressive strain of the concrete ε'_{bu}. From observations on test specimens it was found that $\varepsilon'_{bu} = 0.2\%$ (see Appendix B). The relationship between N' and M can readily

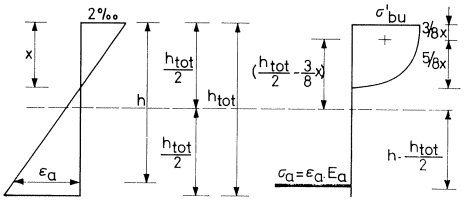

Fig. 46. Determination of M (in relation to middle plane) and the associated N' (normal force).

be determined by calculating the magnitude of N' and M', basing oneself on a particular state of deformation (see Fig. 46).

The resultant moment has been calculated in relation to the middle plane of the slab.

For given slab dimensions and material properties it is, for each slab, possible to calculate the maximum moment in the tangential direction (page 31 and 32).

Values ranging from 1.4 to 2.8, depending on the reinforcement percentage ω_t in the slabs, were found for the ratio $M_{t\max}/M_{t,p}$ (Fig. 44).

Appendix B: Materials

Concrete

It was endeavoured to make a high-strength concrete. A high compressive strength was desired in order to ensure that the steel, not the concrete, would be the deciding factor for collapse of the slab.

Composition

The quantities per litre, allowing for an air content of 1.5%, are as follows:

ENCI Portland cement A	3.85 N
water	1.925 N
aggregate	17.567 N
total	23.342 N

The water/cement ratio is 0.5. The grading curve of the aggregate is presented in Fig. 47.

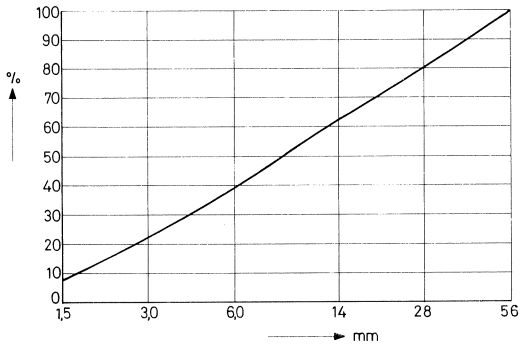

Fig. 47. Grading curve.

Test specimens

Prisms with dimensions of $40 \times 40 \times 160$ mm were made as test specimens for determining the properties of the concrete. Like the model slabs, these specimens were concreted in two layers, each layer being compacted by vibration on a vibrating table. They were then covered with damp cloths and demoulded after three days. On removal from the moulds, the specimens and the model slabs were stored in an airconditioned room where a relative humidity of 90% and a temperature of 20°C was maintained; after two weeks in these conditions the models and the test specimens were stored for a further two weeks in the testing laboratory itself, where they were tested after a hardening period of 28 days in total. Six prisms were concreted along with each slab. Of these six specimens, two were used for determining the flexural strength (σ_b, splitting strength (σ_{sp}) and cube strength (σ'_w), two for determining the prism (com-

pressing strength (σ'_{pr}) and two for determining the stress-strain relationship(σ–ε-diagram).

The flexural tensile strength was determined by means of a three-point bending test. The halves of the specimens subjected to this test were then used for determining the splitting strength and the cube strength (Fig. 48).

The splitting strength was determined by means of the Brazilian splitting test, using 3 mm wide strips inserted between the specimen and the platens of the press (Fig. 48). The rate of loading was 50 N/sec.

For determining the cube strength the load was applied direct through the platens (40 × 40 mm) of the press to the specimens (Fig. 48), as was also done in determining the prism strength and the stress-strain diagram. The rate of loading applied in determining the prism strength and the cube strength was 500 N/sec.

The average stress-strain diagram which was used in the calculations is indicated in Fig. 49.

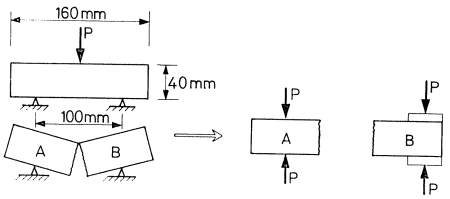

Fig. 48.

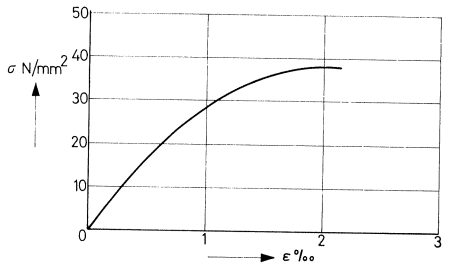

Fig. 49. Average measured stress-strain diagram of the concrete.

The following average values were found for the materal constants of the concrete and used in the calculations:

flexural strength	$\sigma_b = 6$ N/mm²
modulus of elasticity at origin of stress-strain diagram	$E'_{bo} = 34400$ N/mm²
strain corresponding to maximum compressive stress in concrete	$\varepsilon'_{bu} = 0.2\%$
cube (compressive) strength	$\sigma'_w = 50$ N/mm²
splitting (tensile) strength	$\sigma_{sp} = 4.2$ N/mm²
prism (compressive) strength	$\sigma'_{pr} = 37$ N/mm²

Steel (see Fig. 50).

⌀mm	⌀K mm	grade	E_a kN/mm²	σ_{ae} N/mm²	σ_{ar} N/mm²	ε in ‰
2	1,99	Fe B40 HW-NR	199,3	476	568	32
1,6	1,55	Fe B40 HW-NR	199,3	469	573	20
1,4	1,385	Fe B40 HW-NR	200,0	472	566	26,2
1,4	1,385	Fe B40 HK-NR	188,0	438	587	24
1	1,01	Fe B24 HW-NL	–	281	396	57

Fig. 50. Data of the various grades of reinforcing steel.

Appendix C: Formulas for cylindrical orthotropic slabs

The derivation of the *equation for the cylindrical orthotropic slab* is based on the usual assumptions:

- plane sections remain plane and perpendicular to the middle plane;
- the deformations are small in relation to the dimensions of the slab;
- Hooke's law is valid.

Figs. 13 and 51 show the state of stress in an element of the slab.

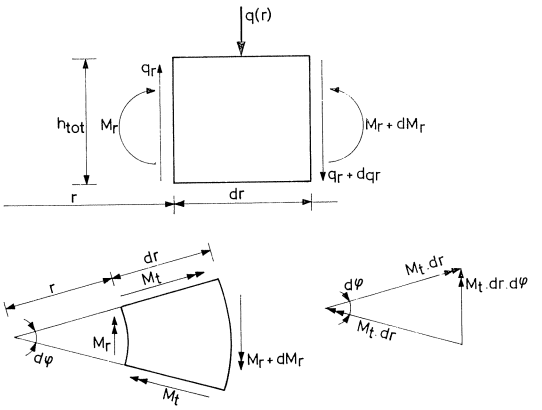

Fig. 51. Forces acting on a slab element.

Because of axial symmetry:

$$q_t = 0$$

$$M_{rt} = 0$$

$$\frac{\partial}{\partial r} = \frac{d}{dr}; \quad r \text{ is the only independent variable}$$

$$\frac{\partial^2 w}{\partial t^2} = \frac{1}{r}\frac{dw}{dr} \quad \text{and} \quad \frac{\partial^2 w}{\partial r^2} = \frac{d^2 w}{dr^2}$$

Deformation equations

Bending moments per unit length:

$$M_r = -k_r\left(\frac{d^2 w}{dr^2} + v_t \frac{1}{r}\frac{dw}{dr}\right) \tag{C1}$$

$$M_t = -k_t\left(\frac{1}{r}\frac{dw}{dr} + v_r \frac{d^2 w}{dr^2}\right) \tag{C2}$$

k_r and k_t are flexural rigidities of the slab in the radial and the tangential direction:

$$k_r = \frac{E_r \cdot h_{tot}^3}{12(1-\nu_r \cdot \nu_t)} \qquad k_t = \frac{E_t \cdot h_{tot}^3}{12(1-\nu_r \cdot \nu_t)}$$

Equilibrium conditions

From a consideration of the equilibrium of an element of the slab (Figs. 13 and 51) the following expressions are obtained:

$$q_r = \frac{dM_r}{dr} + \frac{1}{r}(M_r - M_t) \tag{C3}$$

and

$$\frac{q_r}{r} + \frac{dq_r}{dr} + q(r) = 0 \tag{C4}$$

Equation for the slab

Substitution of (C3) into (C4) gives:

$$\frac{1}{r^2} \cdot M_r + \frac{1}{r}\frac{dM_r}{dr} - \frac{1}{r^2} \cdot M_t + \frac{d}{dr} \cdot \frac{M_r}{r} + \frac{d^2M_r}{dr^2} - \frac{d}{dr}\frac{M_t}{r} + q(r) \tag{C5}$$

Substitution of the deformation equations (C1) and (C2) into the equilibrium equation (C5) gives, in combination with Betti's reciprocity relationship ($k_r \cdot \nu_t = k_t \cdot \nu_r$), the equation for the slab:

$$\boxed{k_r\left(\frac{d^4w}{dr^4} + \frac{2}{r}\frac{d^3w}{dr^3}\right) - k_t\left(\frac{1}{r^2}\frac{d^2w}{dr^2} - \frac{1}{r^3}\frac{dw}{dr}\right) = q(r)}$$

General solution of the slab equation

The equation has been solved by G. F. Carrier (ref. [1]): *particular integral*:

$$w = \frac{q(r) \cdot r^4}{(72k_r - 8k_t)}$$

the *reduced equation* (obtained by replacing the right-hand side by 0) has been solved by the method of changing the variables:

$$t = \ln r$$

$$q(t) = e^{-t} \cdot w(r)$$

The general solution of the slab equation thus becomes:

$(\alpha = \sqrt{k_t/k_r})$:

$$w(r) = A \cdot r^2 + B + C \cdot r^{1+\alpha} + D \cdot r^{1-\alpha} + \frac{q(r) \cdot r^4}{(72k_r - 8k_t)}$$

The constants A, B, C and D are obtained from the boundary conditions of the slab.